The VLT-Astronomical Site Monitor

Commissioning Report

Document No.: VLT-TRE-ESO-10200-1822

Issue 1.1

Date : January 18, 2000

Prepared by: Marc Sarazin

Released by: J. Spyromilio

This page is left intentionally blank

Issue/Rev.	Date	Section/Page affected	Reason/Initiation/Document/Remarks
Prep.1	14.08.98		
1.0	12.04.99	4.2	Added M1 Figuring Errors
		2.3 and 2.5	Updated configuration files
1.1	18.01.00	2.3	added missing dimm mode configuration table

Change Record

This page is left intentionally blank

Contents

List of Tables

List of Figures

1 Documentation

The following documents of the exact issue shown form a part of this specification to the extent specified herein. In the event of conflict between the documents referenced herein and the contents of this specification, the contents of the specification shall be considered a superseding requirement.

1.1 Applicable Documents

-VLT-SPE-ESO-17410-1174	VLT-ASM Seeing and Coherence Monitor, Dimm Upgrade Plan -2.3, Aug.98
-Publication	*The E.S.O Differential Image Motion Monitor* ; Astron. Astrophys. 227, 294-300 (1990)
-VLT-SPE-ESO-17441-1175	Astronomical Site Monitor Control SW Functional Specification - 1.0, Mar.97
-http://archive.eso.org/dicb/DID/	Data Interface Dictionary for ASM provided data ESO-VLT-DIC.ASM-0.2, 06 June98
-VLT-SPE-ESO-17441-1213	Astronomical Site Monitor Control SW Design Description - 1.0/prep.3, 25 Jun.97
-VLT-MAN-ESO-17441-1404	VLT-ASM Control Software, Installation and Operation Manual - 1.0/prep.2, 3 Sep.97
-VLT-TRE-ESO-17430-1270	VLT-ASM Control Hardware, Functional Description - Draft 2, Jan.97
-VLT-TRE-ESO-17430-1271	ASM Control Hardware, Design Description - Draft 3, Mar.97
-VLT-TRE-ESO-17431-1272	ASM LCU, Signal Description - Draft 3, Mar.97
-VLT-TRE-ESO-17431-1273	ASM LCU, Hardware Signal Assignment - Draft 3, Mar.97
-VLT-TRE-ESO-17413-1275	ASM Seeing Monitor, Modification to the motor assembly - Draft 3, Mar.97
-VLT-MAN-ESO-17441-1405	Astronomical Site Monitor DIMM Upgrade Mission - Test Report, 21 Aug.97
-VLT-PLA-ESO-17410-xxxx	ASM Integration and Commissioning: Status January 98 21 Jan.98
-VLT-PRO-ESO-10200-1453	Verification of ASM: Commissioning Test Procedure 2.12.D -1.0/prep.1, 29 May98

1.2 Reference Documents

-VLT-VPO-97/0184	Individual Integration/Commissioning Planning Activities 20 Aug.97, Updated Nov.97
-VLT-DCR-DJO-11710-0000	Small CCD Head Interface -f, Jan.96
-VLT-MAN-DJO-11700-0001	Technical CCD Systems, User Manual -1, May96
-VLT-MAN-ESO-11240-0672	CCD Detectors Control Software, User Manual

	-1.5, 19 Nov.97
-Vaisala Technical Notice	MILOS 500 Automatic Weather Station for the ESO VLT Project
-VLT-SPE-ESO-17410-1253	VLT-ASM Dimm Retractable Enclosure, Functional Specification
	-2.0, Dec.96
	- Nov 97

1.3 Composition of the ASM Team

The VLT-ASM is a two-year project which is now reaching completion. The development of the ASM software, the upgrade of the DIMM, the field tests at La Silla and the integration at Paranal is the work of a small team (R. Amestica, P. Duhoux, J. Navarrete, M. Ravensbergen and S. Sandrock) with the support of the various services of ESO Garching, La Silla and Paranal.

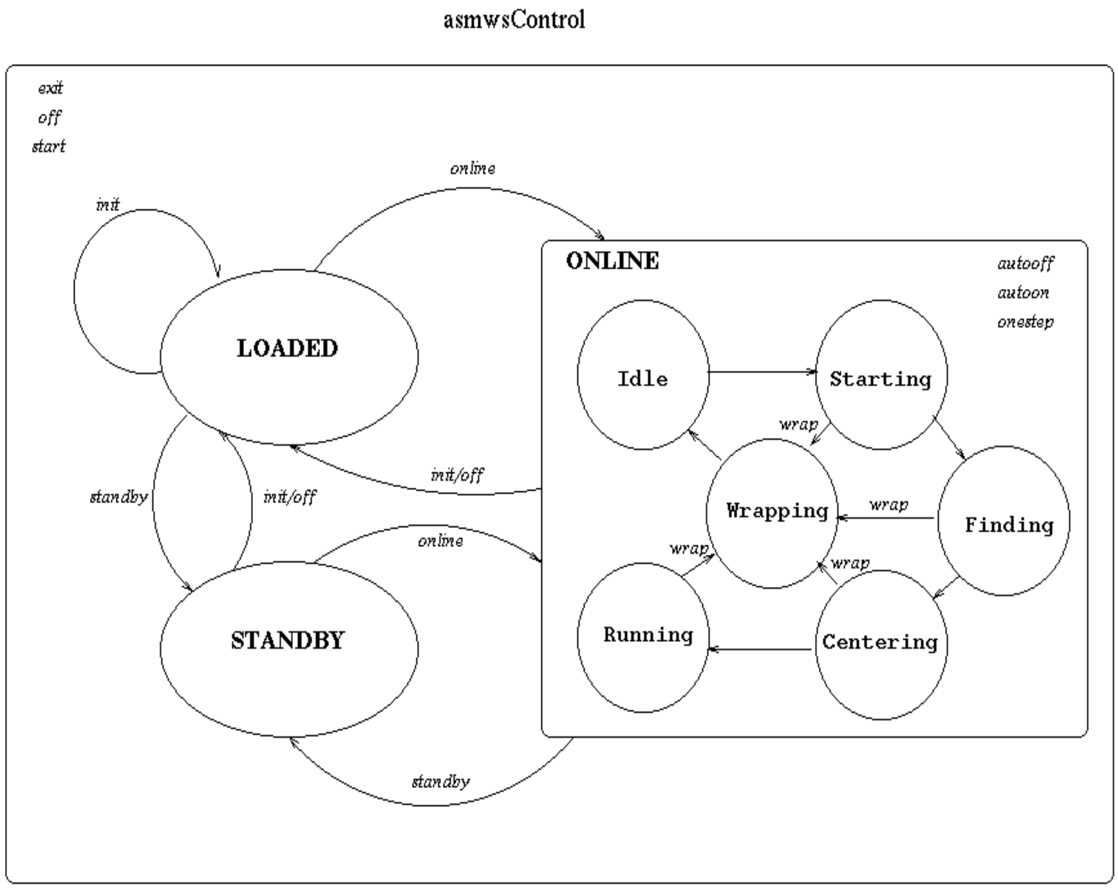

Figure 1: ASM-WS Control Process

2 General Description

2.1 ASM Control Process Description

The ASM is designed as a completely automated system. For this purpose, the various subsystems are controlled by a single process, namely the *asmswsControl* Process running on the ASM Workstation (Figure 1). This process checks for sun position to switch from daytime (STANDBY) to nighttime (ONLINE) states. While in ONLINE state, the control process also takes care of automatic star selection, object centering, autoguiding and measurement (running). In parallel it performs the meteo alarm watch. Sending a *wrap* command during ONLINE operation forces the system to leave its current status and to go back to idle, from there a *standby* command sets the system in daytime mode (dome closed, telescope stopped).

Unattended operation assumes that the main control process never dies. At the time of the present release this is not the case because of a not yet located software error producing memory access faults and causing the process to coredump up to once per night, principally when switching from ONLINE to STANDBY at the end of the night. This problem is under investigation

```
Attribute:  [<alias>asmcat.selection]
       parameter       value       unit
       (0)             (1)         (2)
 0.    Half-sky rest   1
 1.    Hour angle pr   0.5         0..1
 2.    Magnitude pri   0.25        0..1
 3.    Preferred sta   -30000      hhmmss
 4.    Hour angle li   20000       hhmmss
 5.    Maximum airma   2
 6.    Maximum magni   3           mag
 7.    Astronomical    6           deg
```

Figure 2: Star Selection Criteria

2.2 Operational Limits

2.2.1 Meteorology

The current operational limits shown in Table 1 are set in such a way that the DIMM will continue operating after the VLT UTs are closed to assist decision making at time of re-opening. However, the DIMM currently looses efficiency above 15 m/s because of excessive wind shake apparently due to tower lateral oscillation. Plans are being made to stiffen the tower.

Parameter	Limit	Hysteresis
RH	80	5
Wind Gust	21	2
Wind Speed	18	1

Table 1: DIMM Operational Limits

2.2.2 Star Selection

It is foreseen to observe only in the southern half of the sky, the cable paths at the telescope level have not been prepared for a flip-over of the opposite sky half. The positive hour angle limit has been reduced from 3 to 2 hour because of meteorological mast obstruction (Figure 2). The maximum time on the same object is now 5 hours. Astronomical twilight currently set at 6 degrees below horizon defines night and daytime.

2.3 Hardware Constants

The characteristics of the DIMM assembly are stored in a default configuration file loaded when starting the RTAP environment (Figure 3). The configuration should not be changed until the next release. The mode dependent parameters are stored in a separate table shown on Figure 4.

Attribute: [<alias>asmdimConfig.hardware_constants]

	parameter	value	unit
	(0)	(1)	(2)
0.	Telescope Diameter	0.35	m
1.	Telescope F Ratio	15	
2.	Objective Focal Length	0.04	m
3.	Pupil Mask Prism Angle	1.5	degree
4.	Mask Hole Diameter	0.0009	m
5.	Mask Hole Separation	0.0015	m
6.	Pupils Diameter	0.118	m
7.	Pupils Separation	0.197	m
8.	X CCD total size	400	pixel
9.	Y CCD total size	290	pixel
10.	CCD noise floor	-9	A/D count
11.	X Pixel Size	2.2e-05	m
12.	Y Pixel Size	2.2e-05	m
13.	X Pixel Angular Pitch (nom)	0.864	arcsec
14.	Y Pixel Angular Pitch (nom)	0.864	arcsec
15.	X Pixel Angular Pitch (act)	0.884	arcsec
16.	Y Pixel Angular Pitch (act)	0.884	arcsec
17.	Spot Axis Rotation (vs CCD-x)	0	radian
18.	Spot separation (nominal)	45	pixel
19.	Instrumental Noise X (act)	0.007	pixel^2
20.	Instrumental Noise Y (act)	0.007	pixel^2
21.	Wavelength (FWHM)	5e-07	m

Figure 3: ASM hardware constants

Attribute: [<alias>asmdimConfig.dimm_mode_setup]

	parameter	value	unit
	(0)	(1)	(2)
0.	Exposure time	0.005	s
1.	Exposures per frame	1	#
2.	Frames per sequence	800	#
3.	X CCD sub-array siz	40	pixel
4.	Y CCD sub-array siz	40	pixel

Figure 4: ASM DIMM Mode setup

Attribute: [<alias>asmdimConfig.validation_limits]

	parameter (0)	value (1)	unit (2)
0.	Saturation Limit (kr)	3800	A/D count
1.	Valid Pixels Limit (kp)	3	number
2.	S/N Ratio Limit (SNmin)	20	
3.	Spot Elongation Limit (ke)	60	%
4.	Spot Decentering Limit (kf)	2	Spot fwhm
5.	Gaussian Clipping Limit (kc)	3	rms of distr.
6.	Rejected Exposures Limit(kN1)	75	%
7.	Clipped Exposures Limit (kN2)	3	%
8.	Statistical Error Limit (ks)	6	1/sqrt(N-1)
9.	Curve Fit Polynom Order (ko)	2	0=off
10.	Max consecutive rejects (kS1)	10	0=off
11.	Max total rejections (kS2)	30	0=off

Figure 5: ASM Validation Limits

2.4 Automation Subroutines

The functions requested for an automated operation (Object Centering, Autoguiding, Star selection, Sun elevation calculation, Meteo alarms) have been successfully tested.

2.5 Adjustment of variable parameters

Image validation parameters have been adjusted according to the typical image quality provided by this telescope, the final parameter table is given in Figure 5. This configuration should not be modified until the next release.

Each seeing value is computed over 800 short exposures. The time between seeing updates is about 65 seconds. The time elapsed from STANDBY state (dome closed) to the first measurement is 2 minute (presetting not included). The time needed to move from zenith to an object at -3 h hour angle is 2 minute. The dead time without measurements when changing star is at maximum 5 minute.

Attribute: [<alias>asmcat.stars]

	name (0)	info (1)	alpha (2)	delta (3)	magnitude (4)	enable (5)	southern (6)
0.	alf-eri	Achernar	13742.9	-571412	0.46	0	1
1.	alf-car	Canopus	62357.1	-524144	-0.72	0	1
2.	del-vel	delta vela	84442.2	-544230	1.96	1	1
3.	bet-car	Miaplacidu	91312	-694302	1.68	1	1
4.	bet-cru	Mimosa	124743	-594119	1.25	1	1
5.	bet-cen	Hadar	140349	-602223	0.61	0	1
6.	gam-lup	gamma lupu	153508	-411000	2.78	1	1
7.	alf-sco	Antares	162924	-262555	0.9	0	1
8.	alf-tra	Atria	164840	-690140	1.92	1	1
9.	lam-sco	Shaula	173337	-370614	1.63	1	1
10.	sig-sgr	Nunki	185516	-261748	2.02	1	1
11.	alf-pav	Peacock	202539	-564406	1.94	1	1
12.	alf-gru	Alnair	220814	-465740	1.74	1	1
13.	alf-tuc	alpha tuc	221830	-601535	2.86	1	1
14.	alf-psa	Formalhaut	225739	-293720	1.16	1	1
15.	alf-phe	Ankaa	2617.03	-421822	2.39	1	1
16.	NGC-6121	Glob Clust	162335	-263132	6.4	0	1
17.	del-cma	Canis M	70823.5	-262336	1.86	1	1
18.	tau-pup	Puppis	64956.2	-503253	2.93	1	1
19.	alf-col	Columbo	53938.9	-340427	2.64	1	1
20.	alf-hyd	Alphard	15846.2	-613411	2.86	1	1
21.	BSO-18	DBL76.6	84224	-530700	5.3	0	1
22.	BSO-17	DBL65.0	81948	-713100	5.37	0	1
23.	JC-2	DBL268.6	120824	-504300	2.6	0	1
24.	PZ-4	DBL10.4	155654	-335800	5.14	0	1
25.	BSO-22	DBL102.9	162018	-784200	4.68	0	1
26.	DUN-126	DBL34.9	125436	-571100	4.03	0	1
27.			0	0	0	0	0

Figure 6: ASM Star Catalogue: only enabled objects are used for seeing measurements

3 Telescope Performance

3.1 Pointing Model Performance

From offset coordinates measured in the final mount position on several objects in the southern half-sky, the pointing model parameters were computed using T-Point. Presetting is then accurate enough for all objects in the ASM catalogue (Figure 6). An additional feature of spiral search has been successfully introduced for finding objects outside the working area (eg. for double star calibration).

3.2 Telescope Tracking

The autoguiding integral and proportional gains have been adjusted to filter out wind shake (Figure 7). However periodic tracking errors cannot be compensated by autoguiding (Figure 8). The ETA axis behaviour is quite satisfactory (± 0.5 arcsec error). A fine tuning of the THETA axis server parameters could possibly reduce the ± 2 arcsec excursion, this is to be investigated.

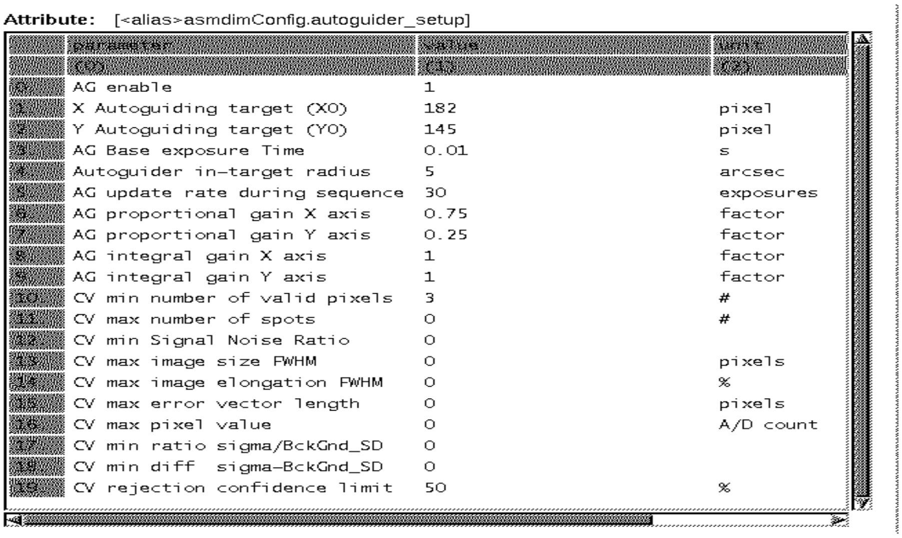

Attribute: [<alias>asmdimConfig.autoguider_setup]

	parameter (0)	value (1)	unit (2)
0	AG enable	1	
1	X Autoguiding target (X0)	182	pixel
2	Y Autoguiding target (Y0)	145	pixel
3	AG Base exposure Time	0.01	s
4	Autoguider in-target radius	5	arcsec
5	AG update rate during sequence	30	exposures
6	AG proportional gain X axis	0.75	factor
7	AG proportional gain Y axis	0.25	factor
8	AG integral gain X axis	1	factor
9	AG integral gain Y axis	1	factor
10	CV min number of valid pixels	3	#
11	CV max number of spots	0	#
12	CV min Signal Noise Ratio	0	
13	CV max image size FWHM	0	pixels
14	CV max image elongation FWHM	0	%
15	CV max error vector length	0	pixels
16	CV max pixel value	0	A/D count
17	CV min ratio sigma/BckGnd_SD	0	
18	CV min diff sigma-BckGnd_SD	0	
19	CV rejection confidence limit	50	%

Figure 7: ASM Autoguider configuration

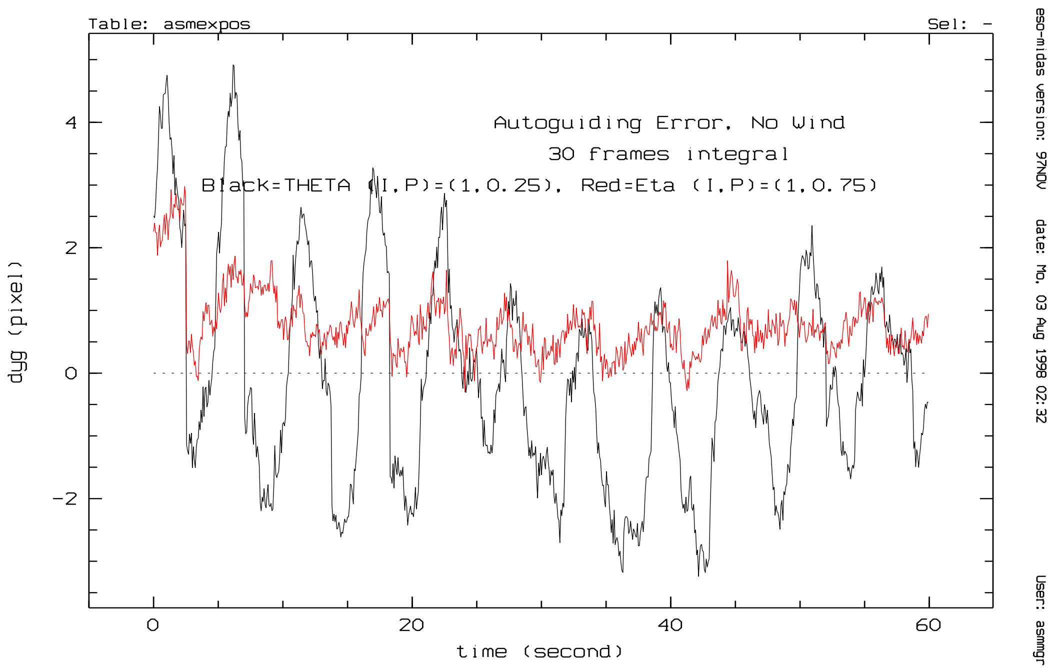

Figure 8: ASM Autoguider Performance

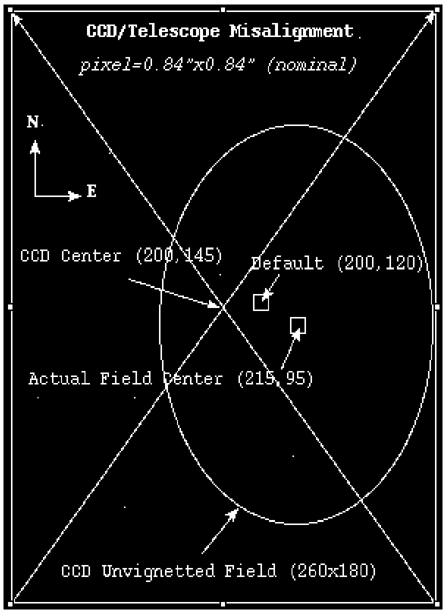

Figure 9: ASM Field Misalignment

4 Optical Quality

4.1 Field Alignment

A misalignment of the telescope or of the pupil imaging optics leads to a reduction of the unvignetted observation field (Figure 9). After proper alignment of the relay optics and detector, 90% of the detector area can be used for finding the objects.

4.2 Coma Alignment

The alignment configuration is obtained by moving the transfer optics out of the light path and pushing the cassegrain focus until the defocused image of the pupil fits completely inside the detector area. Then the standard procedure of moving M2 in tilt and translation is employed, until the pupil image is centered and circular.

M1 high spatial frequency figuring errors are visible on a defocused image after optimal coma alignment (Figure 10). These are responsible for the sup-pupil image elongation and secondary maxima chown on Figure 13.

4.3 Full Pupil Imaging

Removing the beam splitting prism from the optical path, the full 35 cm pupil of the telescope can be used for imaging and image quality is then limited by the atmosphere. A correct imaging quality is achieved with exposure time up to 5 s without autoguiding (Figure 11). With longer exposure time, image elongation is visible due to the THETA axis tracking error.

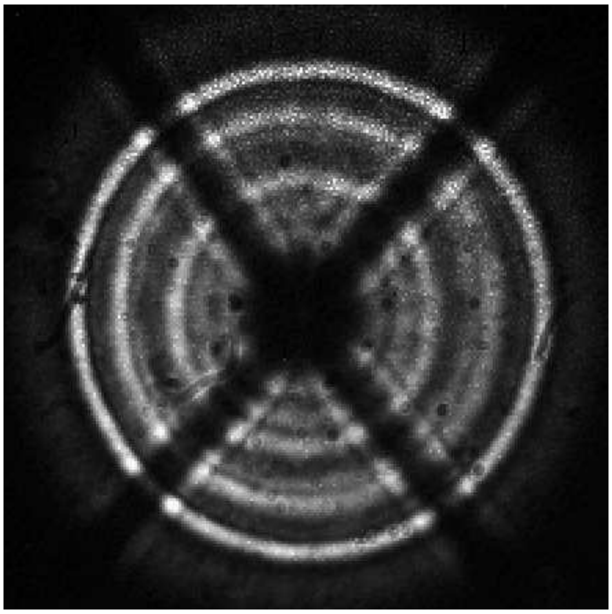

Figure 10: M1 (F/2 parabola) high spatial frequency figuring errors

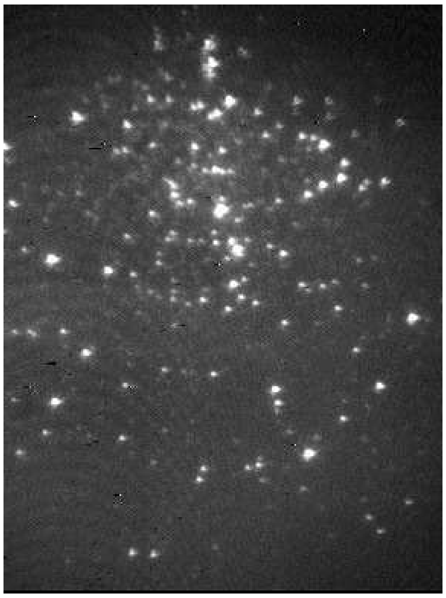

Figure 11: ASM Optical Quality: NGC-6121, 5 s exposure, Aug. 6 00:48, seeing=0.8", no bias subtraction

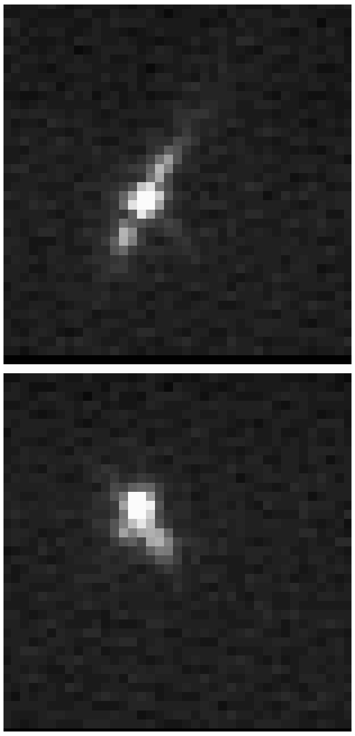

Figure 12: ASM Sub-Pupil Imaging

4.4 Sub-Pupil Imaging

With the beam splitting prism and pupil mask installed and in good seeing conditions, the images present a clear diffraction pattern (Figure 12). The secondary maxima are about 25 times less intense than the central core (Figure 13) and are thus partially taken into account during centroid calculation on bright objects. The asymetry of the diffraction pattern may thus introduce a noise term variable with the position in the field which is partially removed by the least square subtraction described in section 5.5. The relative importance of this noise term will be investigated once a large enough database is accumulated with the current setup, comparing measurements on faint and bright objects.

4.5 CCD Photometry

The Stellar flux is computed from the difference of the total illumination over the sub-array to the total average background. The image background is measured on the three least illuminated corners of size one quarter of image side (ie. 10x10 pixels for a 40x40 window). Accurate photometry needed for measuring atmospheric extinction can only be achived which a stable detector response. As shown on Figure 14 the current TCCD fast read-out in windowing mode produces changes in the chip internal temperature which changes the amplifier response. This problem is under investigation. A degraded sky monitor mode with transparent Cirrhus detection is nevertheless possible in the current situation.

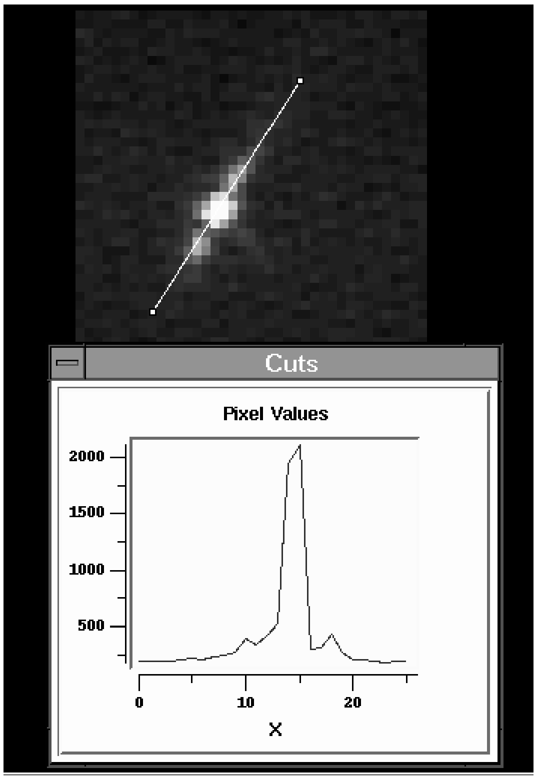

Figure 13: ASM Sub-Pupil Cuts

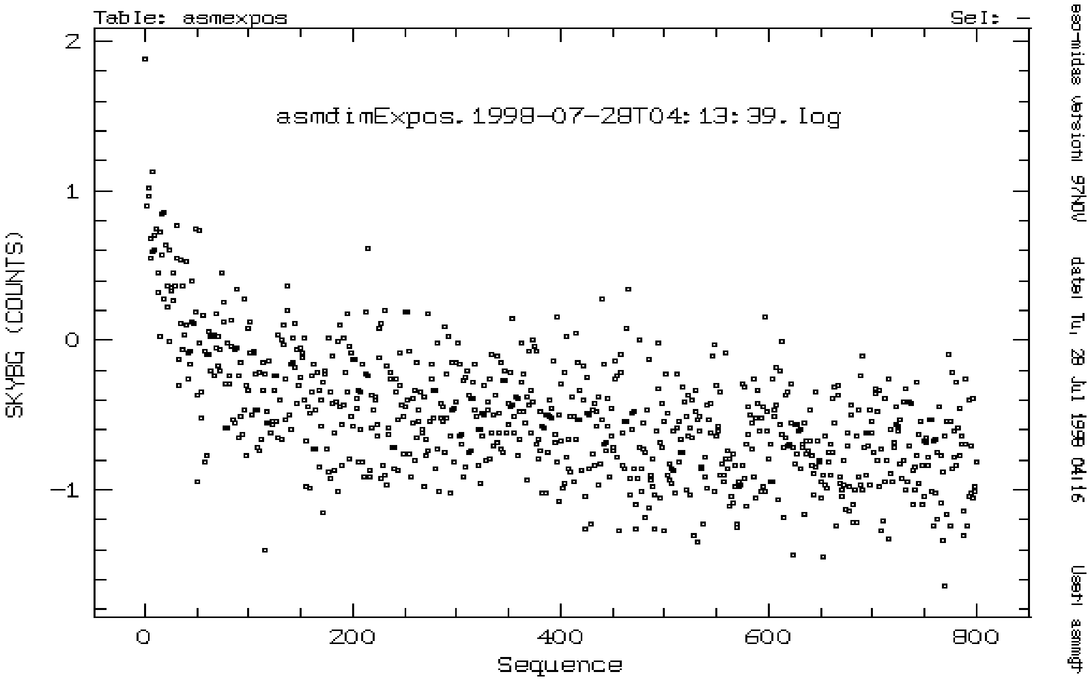

Figure 14: TCCD Background Variation in the course of a sequence of 800, 5 ms exposures after bias subtraction

4.6 Centroiding Method

Only a selected number of pixels are used to compute the centroid, according to their illumination. In the previous versions of the DIMM, the selection criterium was chosen as a fraction of the maximum in the image. In this release, the standard TCCD autoguider software algorithm allows for selecting pixels above a multiple of the RMS background level measured as described in section 4.5. This has the advantage of making possible to compute the centroid of speckled images when using very short exposure time as in the coherence mode. This has the drawback described in section 4.4 of loosing control on the contribution of asymetric diffraction patterns to the centroiding error. The highest allowed threshold was chosen (9 times the RMS background) to minimize this effect.

5 Error Budget on Seeing Measurements

5.1 Summary

The goal is to maintain an accuracy better than ± 10 % down to 0.25 arcsec seeing. At such a low seeing value, the instrumental noise contribution (Section 5.3) is dominating with a value of $\pm 8\%$ per way (Figure 18), or $\pm 6\%$ on the average. At higher seeing values, the overall accuracy is of the order of $\pm 5\%$

5.2 Statistical Error

The relative error on the average variance of the differential motion in each direction of measurement is expressed as $\frac{2}{\sqrt{N-1}}$ where N is the number of samples in the time serie. The corresponding error on the directional seeing is 3/5th of this value, thus varying from $\pm 3\%$ when all 800 images of the sequence are validated (normal operation) to $\pm 6\%$ when reaching the validation limit of 200 exposures (clouds or high wind). The seeing average over the two directions of measurement has a statistical noise reduced by $\sqrt{2}$, thus of the order of $\pm 2\%$ in normal operation. As shown on Figure 15, the natural anisotropy of the atmosphere is twice the 800 exposure statistical error, ie: of the same order as the 200 exposures statistical error which is chosen as validation limit.

5.3 Instrumental Noise

The estimate of this noise term is of prime importance for achieving high accuracy at low seeing values: a double star simulator has been designed for this purpose. The camera is removed from the telescope and installed in the image plane of the simulator. The system is set in measurement mode without any change in the operational configuration. The variance of the differential motion measured on such non-moving objects constitutes the so-called instrumental noise (Figure 16). It takes into account all detector dependent noise sources (intrapixel quantum efficiency variation, photon noise, undersampling) as well as pure centroiding error. It is measured with various illumination levels and image sizes representative of operational conditions, but without motion over the detector and without asymetrical diffraction patterns.

The instrumental noise is completely decorrelated from the relative motion due to the atmosphere. It is thus additive and can be subtracted out from the variance before seeing computation (Figure 17).

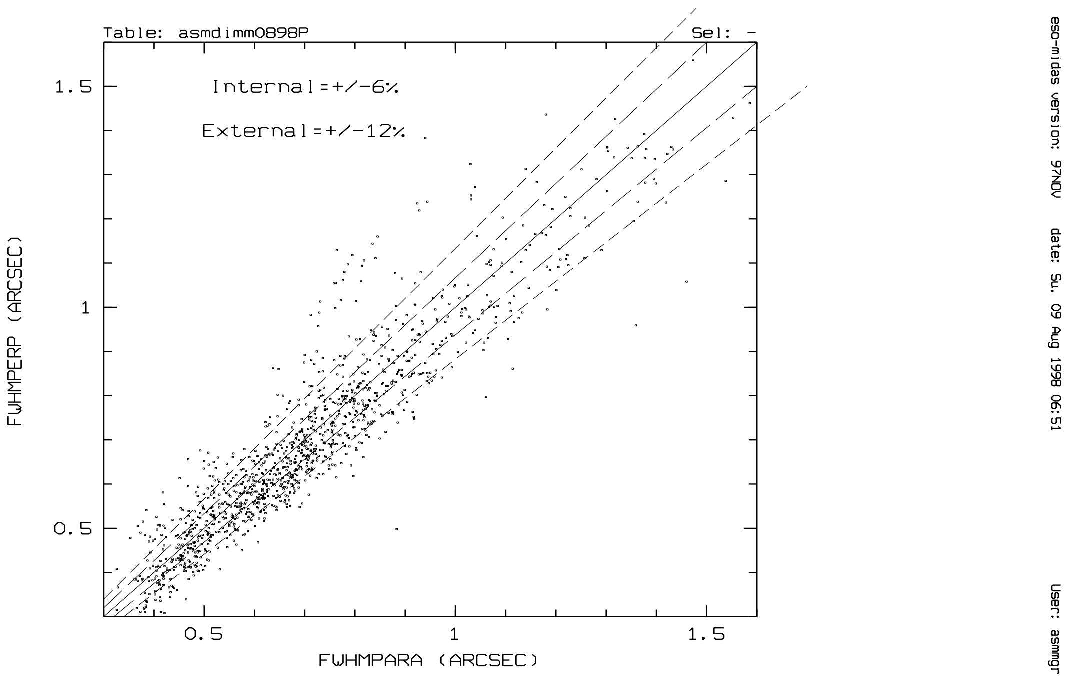

Figure 15: ASM Statistical Noise and Natural Anisotropy

The DIMM accuracy is then limited by the stability of this noise term. In the present case, the error on the noise is estimated to ± 3 RMS or ± 0.002 Pixel^2. The relative contribution of this term to final seeing is given in Figure 18 in the most sensitive case of the perpendicular motion.

It is foreseen to continue investigating the instrumental noise, and in particular to compare the measurements to the results of a theoretical model.

5.4 Absolute Plate Scale Calibration

Imaging a double star with the beam splitting prism and pupil mask installed is quite straightforward (Figure 19). However the incidence angle on the prism is not normal anymore, introducing some additional deflection of the images. It is thus more accurate to measure pixel scale without prism (Figure 20). The object separation can be measured a posteriori using standard image processing tools (Figure 21) such as MIDAS CENTER/GAUSS command. However and even more convenient method is to let the system run in DIMM mode on the double star image without prism (Figure 22). The seeing measured in this case is not the atmospheric seeing but rather an expression of the wavefront tilt anisoplanatism (the ASM public data switch shall be disabled during calibration operations).

The atmospheric seeing is obtained from the 3/5th power of the variance, thus varying as the 6/5th power of the pixel size. The error on the pixel scale determination leads to a 1.2 times larger error on the seeing. Although the measurements presented on Figure 22 indicate a negligible error on the absolute plate scale measurement with the double star DUN-126 (sep=34.9"), the same data taken on another double star of larger separation (BSO-22, sep=102.9") return a value lower by 0.5% (0.875 arcsec per pixel). Such a difference is only partly explainable by field curvature effects. The remaining has to be attributed to the accuracy on the separation given by the catalogue (VizieR). We will assume conservatively that the pixel size is known with an accuracy of ± 1 % and we choose the value given by the double star of smaller separation (DUN-126, Figure 22) having smaller field

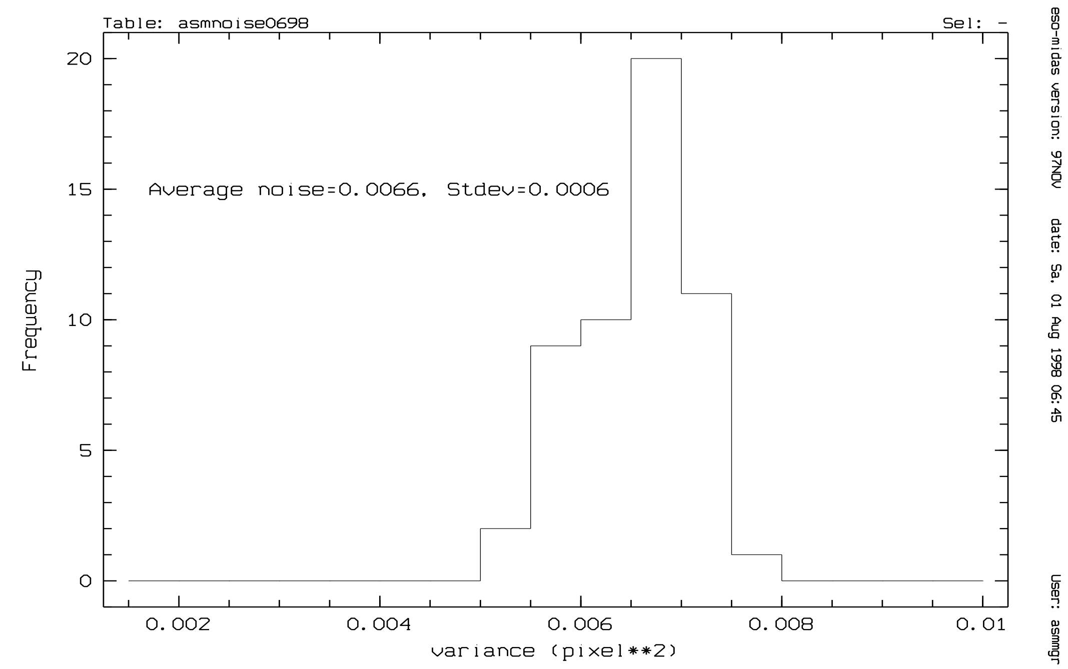

Figure 16: ASM Instrumental Noise Measurement

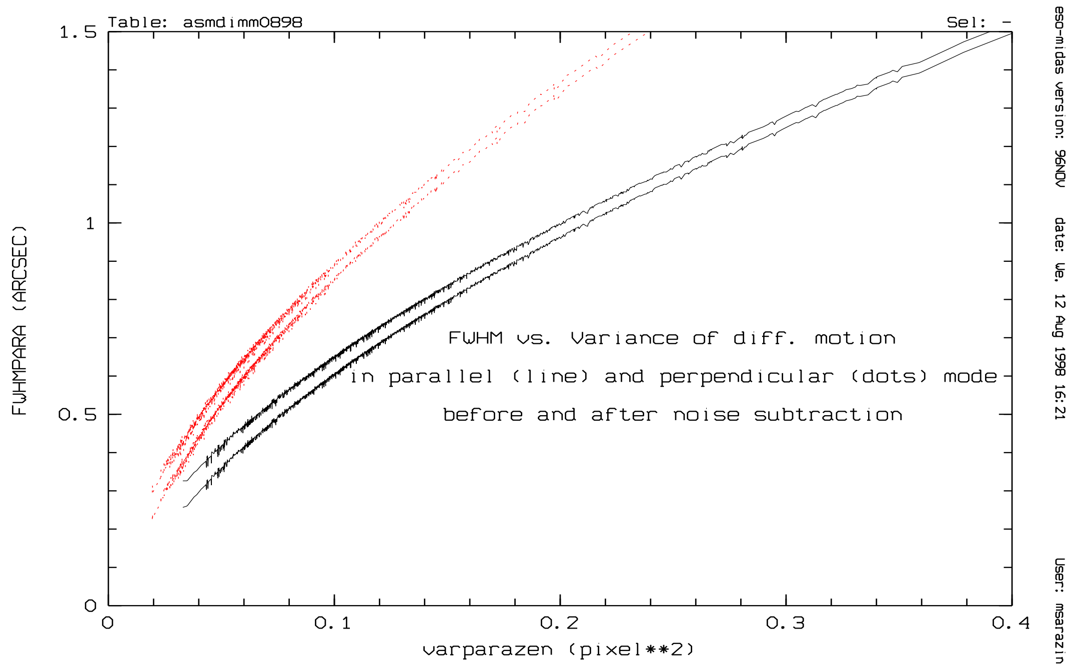

Figure 17: ASM Instrumental Noise Subtraction

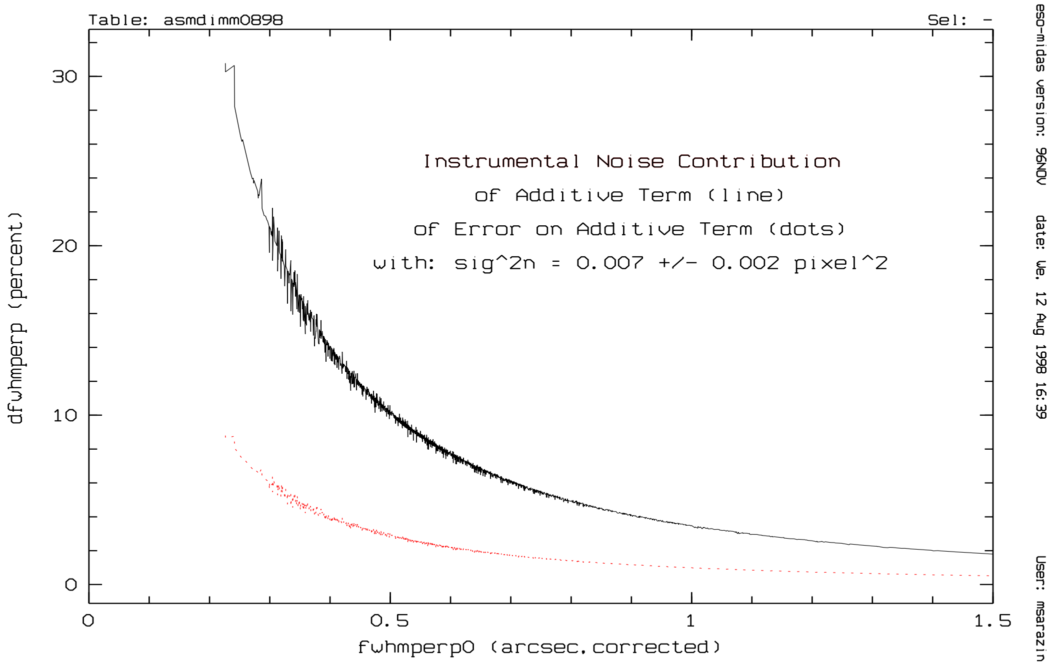

Figure 18: ASM Instrumental Noise Contribution

curvature effect.

5.5 Field Distorsions

Variations of image profile with field position are due to telescope misalignment and to a lesser extent to the asymetry of the diffration pattern. Such effects can be detected in the analysis of the distribution of the differential image motion in both directions with respect to the autoguiding errors in the corresponding axes. Any detectable trend can be only caused by instrumental errors. The ASM software provides for polynomial fitting and removal of this effect. The amount removed should be as small as possible in a well aligned instrument. With the current system, the relative contribution of the least square removal amounts to less than 1% independently of seeing conditions (Figure 23). The long term monitoring of this parameter is a fair check of instrumental quality.

6 Data Verification

6.1 Effect of observation aimass

A whole night was used to demonstrate the robustness of the seeing measurement with respect to observing direction and zenith angle as shown on Figure 24 by switching from one object of the catalogue to the other very frequently.

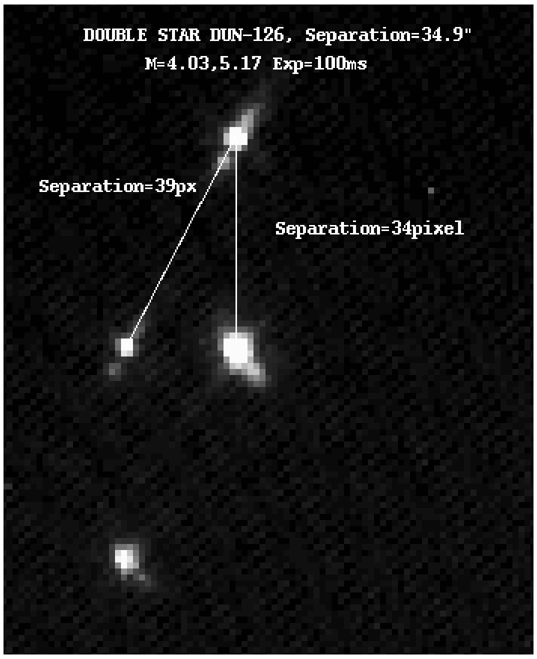

Figure 19: ASM Plate Scale Calibration Image with Prism

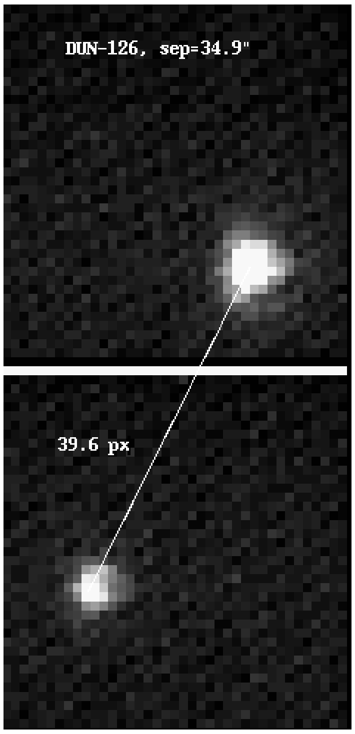

Figure 20: ASM Plate Scale Calibration Image Full Pupil

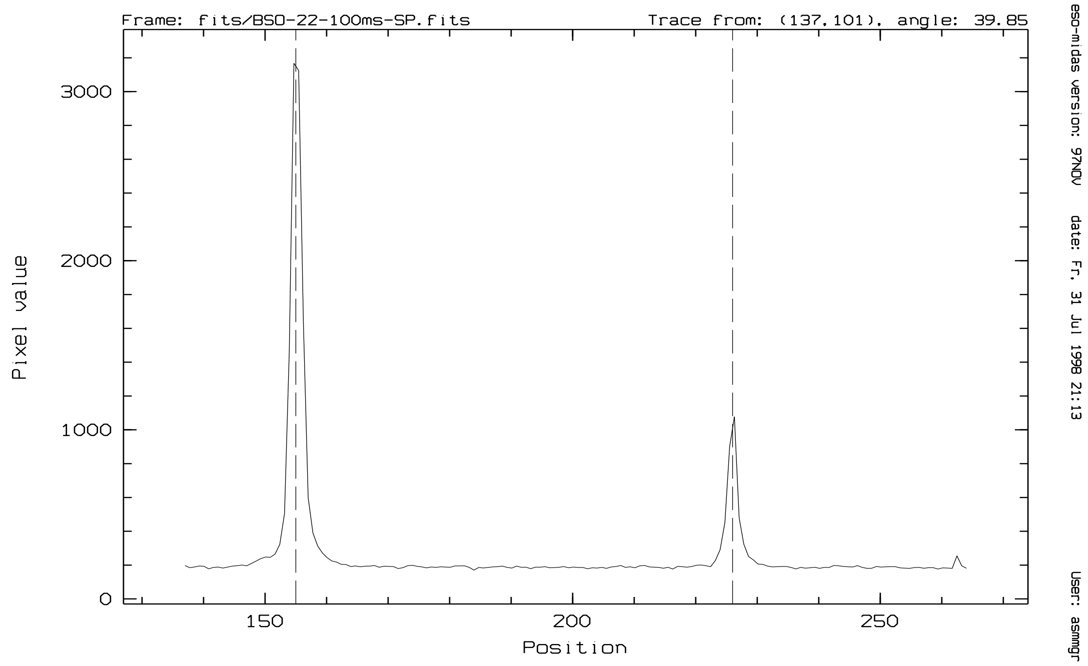

Figure 21: ASM Plate Scale Calibration Cuts

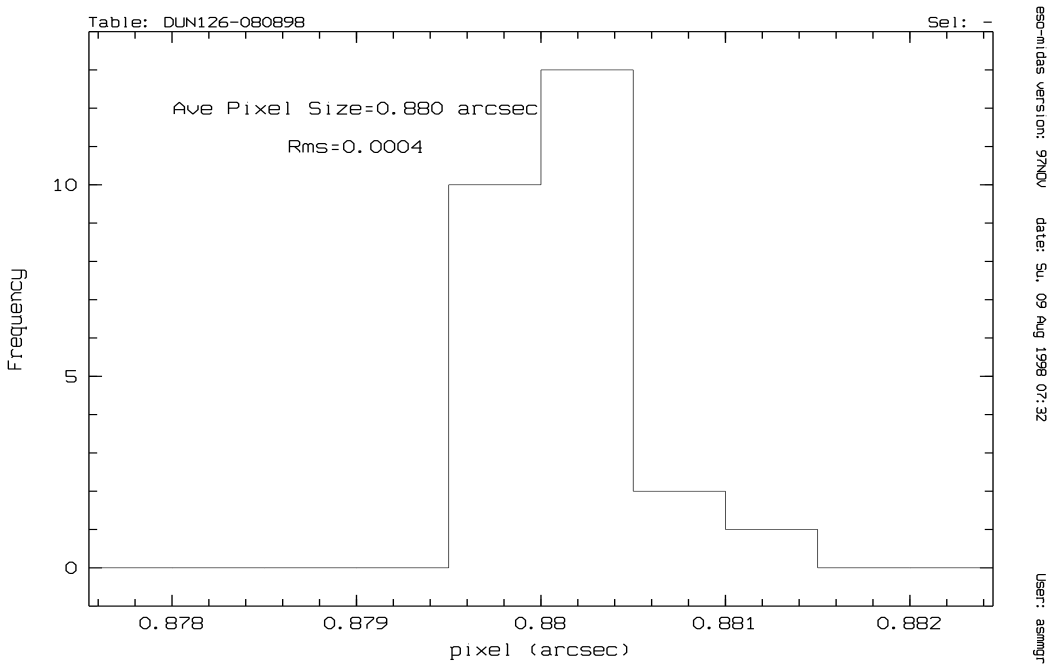

Figure 22: ASM Plate Scale Result

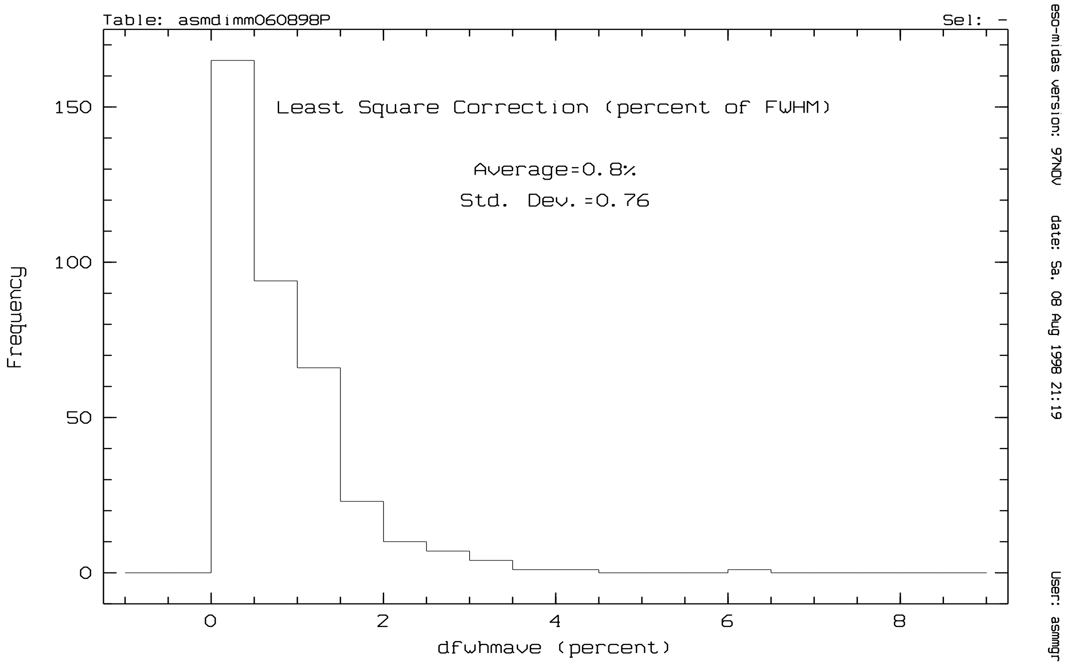

Figure 23: ASM Least Square Correction for field distorsion

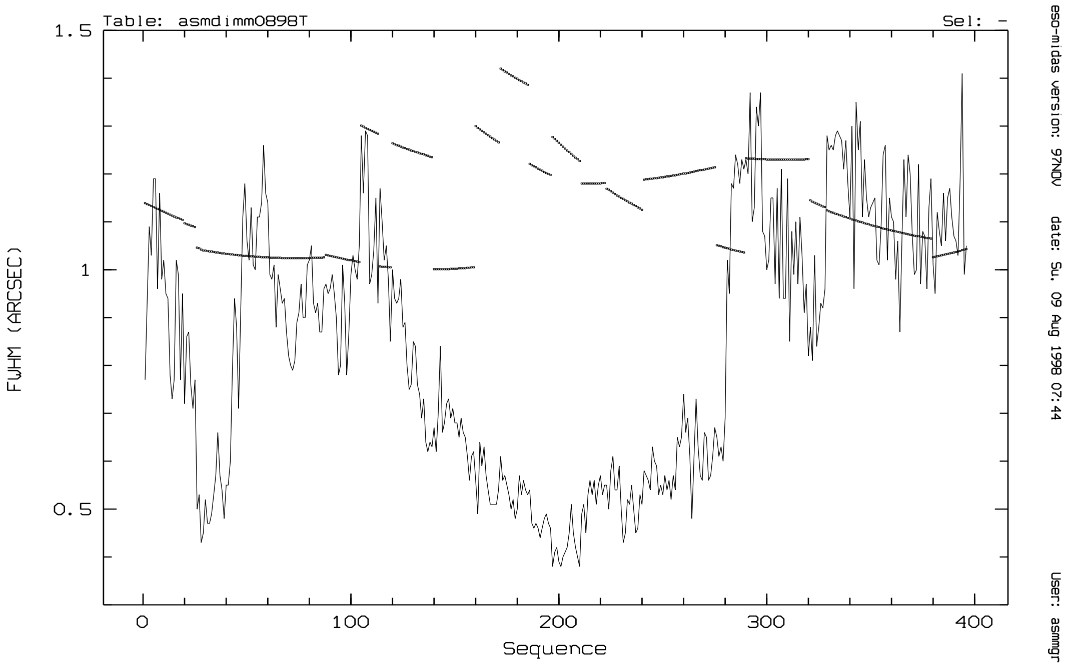

Figure 24: Seeing Measurements (full line) with varying Airmass (dots)

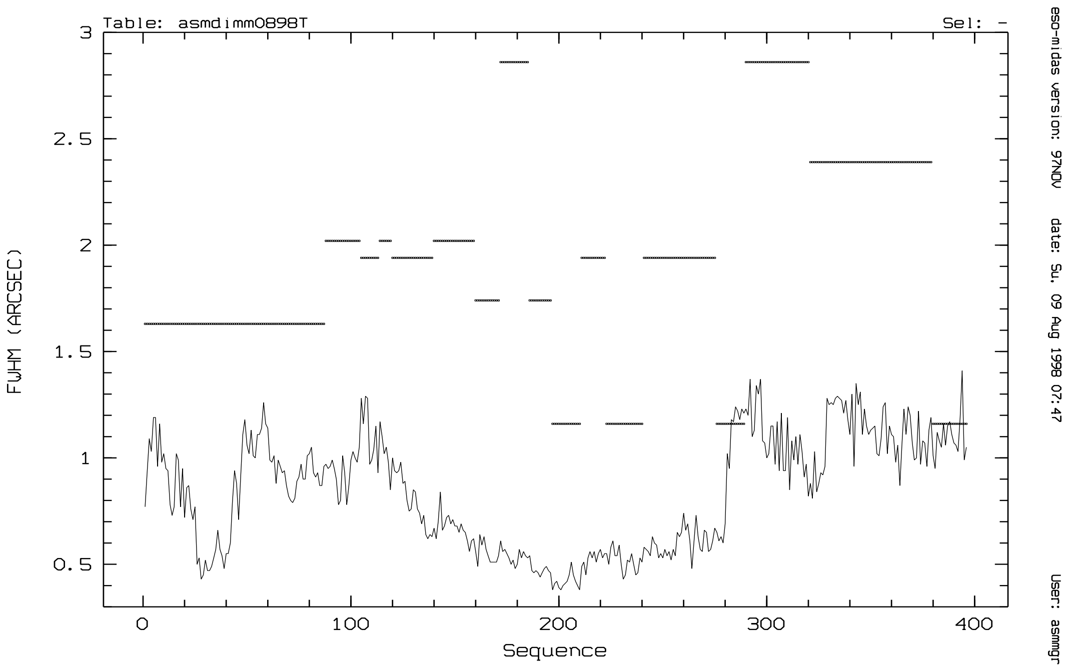

Figure 25: Seeing Measurements (full line) with varying Magnitude (dots)

6.2 Effect of object brightness

A whole night was used to demonstrate the robustness of the seeing measurement with respect to object brightness as shown on Figure 25 by switching from one object of the catalogue to the other very frequently.

6.3 Effect of wind

The relative variation of the number of seeing estimates produced per hour during the first two nights after commissioning as a function of wind velocity shows a correct behaviour up to 12 m/s.

Figure 26 is the first of a long serie of efficiency analyses to be made during permanent ASM operation. Even when fully automated, the ASM data quality will be monitored continuously. A series of tools will be developped for this purpose.

7 Conclusion: Access and Use of ASM data

7.1 Display and Archiving

An online display of meteo and seeing data is provided at the UT contol room using RtapPlotDisp tool. Two classes of ASM parameters are logged in the ESO archive and defined in the DIC.ASM dictionary: the *public* data (18 meteo and seeing parameters of the class cond-log) and the *engineering* data (150 parameters of the class ops-log describing the instantaneous status of all ASM subsystems).

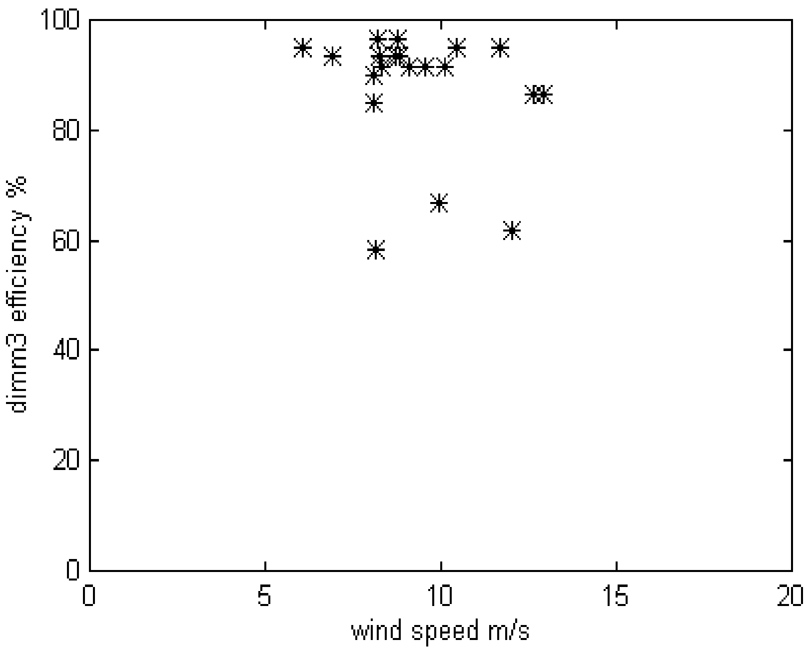

Figure 26: DIMM efficiency per hour as a function of wind velocity during the nights following commissioning. The 3 lower bins are due to software failure (LCU reboot).

7.2 Precaution when using DIMM seeing data

The DIMM was designed as a tool for optimizing queue management in flexible scheduling mode. It is however also extensively used to control the overall UT efficiency with respect to optical alignment and locally generated turbulence. To prevent any misleading conclusions, comparing UT images to DIMM data should follow strict rules, some of them listed below:
-use UT 'long exposures', ie: longer than 30 second
-convert DIMM data (given at AM=1) to UT observing airmass multiplying DIMM data by $(\text{airmass})^{0.6}$
-convert DIMM data (given at 0.5μm) to UT observing center wavelength multiplying DIMM data by $(0.5/\lambda)^{0.2}$
-rebin DIMM data to the exact time span of UT exposure: as shown on Figure 27, the larger the exposure time, the more the natural atmospheric random behavior is averaged out.
-finally keep in mind that 8m class telescopes have reduced image motion due to the finite nature of the outer scale of the turbulence, leading to an improvement of up to 10% compared to DIMM data, depending on atmospheric conditions

8 APPENDIX: Tasks Summary

8.1 Pending short term for October Release

-Monitor closely the behaviour of the ASM with respect to changing observing conditions [JNA]
-Make ccseiMsg STATUS information more explicit: automatic operation is reported ON when using FIXSTAR. This is misleading because sun position and meteo limits are not checked. Automatic operation should be ON only when the system is completely autonomous [RAM].

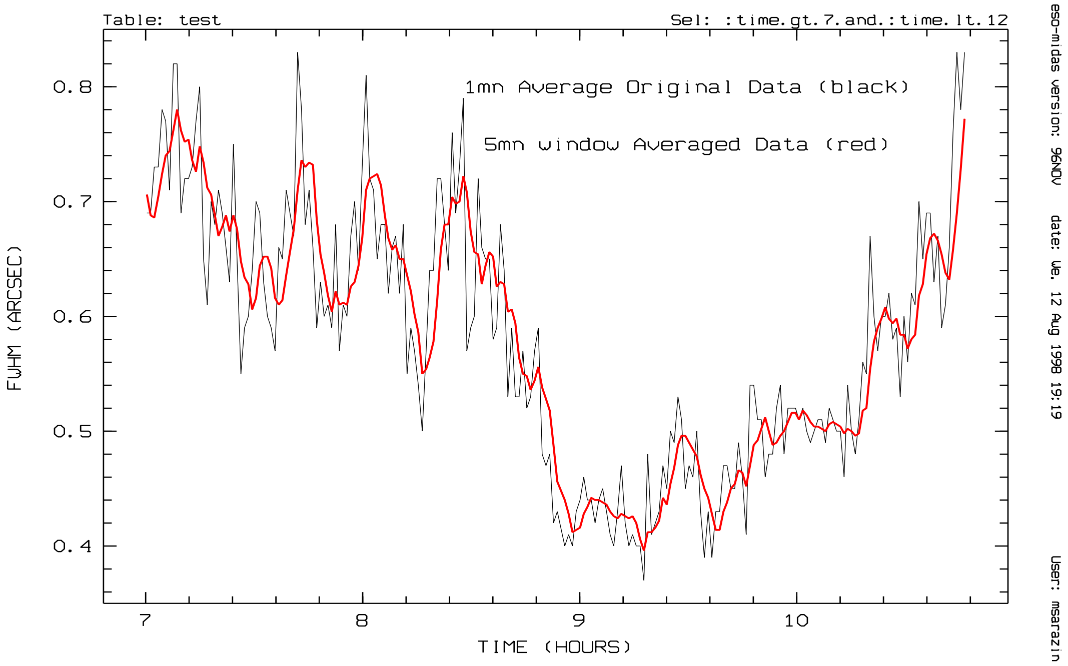

Figure 27: Time Averaged and Original Seeing Measurements

-Analyze the stability of CCD response in windowing mode as a function of frame index and window size [PDU+RRE]. Because of the variation of the background, bias cannot subtracted for centroiding (otherwise leads to negative values). SNR computation as currently defined is then of little use. However, this has no effect on centroiding accuracy.
-Update pointing model: after optical re-alignment, most objects fall ca. 1 arcmin to the West. Adjust centering parameter so as to reach target in a softer way when coming from far away [JNA+RAM].
-Implement the line of sight sky monitor function [SSA+RAM+MSA]
-Enable the three corners background measurement in static thresholding as well (currently only used in dynamic mode) [RAM]
-Deliver average scintillation for zenith rather than for line of sight, ie. multiply by $\cos\gamma^{\frac{11}{6}}$.
-Find reason for, and eliminate (!) sporadic coredumps related to event handler in the ASM main control process [RAM+VLT software group].
-Implement checking for moon position and phase into the automatic selection of stars from the DIMM catalogue.
-Increase axis servo-loop delay from 5 to 10ms to reduce load of telescope LCU if deemed necessary [RAM].
-Update documentation [SSA+RAM+MSA].
-The 220V power cable should be moved away from the ACE 24V cable in the cable duct from the ASM control room to the telescope tower [GHA].

8.2 Pending medium term

-Get time bus from UT1 to TCCD LCU (additional boards ordered by UT1).
-Get cooling fluid to ASM (currently using stand-alone chiller) [AIV].
-Replace plastic encoder plugs (on telescope motor side) by heavy duty connectors [GHA].

-The vibration modes of the DIMM tower were measured [BKO+FKO]. The 8Hz eigen frequency of the tower is responsible for excessive star wandering in high wind condition. The tower will be stiffened according to calculation to be done by [FKO].
-Design wind screen for DIMM telescope if deemed necessary after tower has been stiffened [MQU].
-Investigate reason for X-shaped stray light pattern in the DIMM images.
-Provide new prism with larger angle allowing for larger windows on the CCD and thus fewer frame rejection in high wind condition [MSA]

8.3 Closed Items

-Pointing of telescope is correct: uses standard T-Point model (successful in the standard operation field) + spiral search algorithm (100% hit rate all over the sky)
-Tracking of telescope is correct: pointing model is disabled during tracking to prevent divergence when passing close to zenith. Tracking error with autoguiding is ± 0.5 arcsec in ETA and ± 2 arcsec in THETA (periodic)
. -Telescope optical alignment is complete. Measurements can be performed on objects down to 4th magnitude with an exposure time of 5 ms. With objects brighter than magnitude 1, a X shaped stray-light pattern is visible.
-Absolute plate scale of 0.88 arcsec per pixel has been measured using double stars of known separation.
-Centroiding is now using dynamic thresholding (threshold is calculated on each frame as a multiple of the rms background of the three non illuminated corners of the image). Bias subtraction is used for centering, but not during measurements. The measurement area chosen (set point 182,145) is void of cosmetic defects.
-Least square fitting of differential motion time series and slope removal before variance calculation to account for unwanted field effects.
-Meteo control process checks for message consistency before releasing data to public.
-Enclosure is set to standby (closed) in case of fatal error events in other subsystems (an error message is also logged to TCS requesting maintenance). In addition, the software will not try to open the enclosure when the light sensor is activated.
-Telescope control process now traps low amplitude encoder response during presetting (prevents telescope crash in case of encoder read-out failure).
-One reason for telescope LCU hanging has been eliminated: tLogTask set to priority 1 to prevent queue overflow.
-Autoguider now using proportional integral algorithm to reduce overshoot in high wind conditions. Coefficients have been tuned with 15 m/s wind.
-Flag installed in configuration file to disconnect the ASM from public data during maintenance and trouble-shooting activities.
-The ACE box was shielded but without effect on the persistent moire noise pattern. A threshold of 9xrms background was set to eliminate this pattern from centroid computation.
-The fiber link of the time bus from UT1 to DIMM telescope LCU was properly installed into cable ducts.
-The failing GILL ultrasonic 3D anemometer is now working. The cause was an improperly grounded 24V power supply.